

Original Research

The Potential Distribution of Rice Water Weevil (*Lissorhoptrus oryzophilus*) in China under Current and Future Climatic Conditions

Wenqi Xie^{1#}, Xueyan Zhang^{1#}, Rulin Wang², Yue Zhang¹, Maryam Mumtaz¹,
Qing Li¹, Chunxian Jiang^{1*}

¹College of Agronomy, Sichuan Agricultural University, Chengdu, Sichuan, 611130, China

²Sichuan Provincial Rural Economic Information Center, Chengdu, Sichuan, 610072, China

Received: 30 April 2022

Accepted: 16 July 2022

Abstract

As an agricultural pest, the rice water weevil (RWW), *Lissorhoptrus oryzophilus*, poses a severe threat to agriculture in China. This study aimed to predict the suitable distribution of the RWW in China under current and future climatic conditions based on MaxEnt model with tuning parameters. The results showed that the dominant environmental variables that influenced the geographic distribution of RWW were temperature seasonality (Bio4), mean temperature of the coldest quarter (Bio11), precipitation seasonality (Bio15), and precipitation of the warmest quarter (Bio18). Under the current climatic conditions, the total suitable area of RWW in China was 391.0698 million hm², accounting for 40.77% of China. These suitable areas were mainly located in eastern China, central China and southern China. There was considerable overlap between the suitable areas of RWW and rice cropping regions in China. Under future scenarios, the highly suitable areas for RWW would increase significantly. The centroid migration in the suitable areas of RWW showed a trend of moving eastward and northward. The results of this study can provide theory and data support for the monitoring, early warning and control of RWW.

Keywords: rice water weevil, *Lissorhoptrus oryzophilus*, potential distribution, climate change, MaxEnt

Introduction

Rice water weevil (RWW), *Lissorhoptrus oryzophilus*, is a destructive pest of rice belonging to Coleoptera, Curculionidae, Erihinae, and *Lissorhoptrus*. RWW is listed by the International

Union for Conservation of Nature as one of the 100 most threatening invasive species worldwide [1, 2]. In China, RWW is listed as a national agricultural plant quarantine pest. Adult RWW feed on the leaves of rice plants, leaving narrow feeding scars parallel to the venation of the leaves. The larvae feed in the roots of rice or directly bite off the rice roots [3-5]. The damage caused by RWW to rice reduces yield by 20%~30% [6]. It is a great threat to rice production in China.

Wenqi Xie and Xueyan Zhang are the co-first authors.

*e-mail: chunxianjiang@126.com

RWW originated in the Mississippi River valley of south-central North America. It had spread to North America, Central America, South America, Asia and Europe [7-10]. In China, it was first discovered in Tanghai County, Hebei Province, in 1988, and it gradually spread throughout the country [11]. The spread of RWW in China can be divided into two stages: the sporadic spread stage from 1988 to 1996 and the distribution of RWW concentrated in Bohai Bay and the southeastern coastal area. Since 2001, it has been spreading rapidly from coastal areas to inland provinces [12]. By 2021, RWW had spread to 450 counties in 25 provinces in China [13]. Considering its rapid spread, we should pay more attention to the monitoring and control of RWW.

The supercooling point of overwintering RWW adult is $-15.3\sim-21.2^{\circ}\text{C}$, and the freezing point is $-14\sim-18.6^{\circ}\text{C}$, demonstrating the resistance of RWW to intense cold. When the temperature rises above 10°C in early spring, overwintering adult begin to revive. When the temperature rises above 15°C , diapause terminates, and they begin to feed [14-16]. From mid to late April, they gradually move to rice seedling fields or the weeds beside ditches. From late April to early May, immediately after early rice transplanting, they begin to migration to the paddy field. Annual temperature changes cause the migration peak of overwintering adults to vary. In particular, the impact of precipitation on temperature significantly affect the main migration peak in April and May [17]. Therefore, temperature and precipitation are two important factors affecting the activities of RWW.

Potential distribution analysis, especially scientifically predicting the potential area and spread trend, is a prerequisite for the risk assessment, rational quarantine measures and scientific control of a pest [18]. The CLIMEX, ArcView and MaxEnt models were used to predict the suitable area of RWW in China [12, 19, 20]. However, RWW has continued to spread in China. The latest distribution of RWW indicated a significant change.

Due to the continuous increase in CO_2 and other greenhouse gas emissions and the impacts of human activities, the trend of global climate change has become more obvious. Insects are poikilotherms, and global climate change has both direct and indirect impacts on their growth and development, metabolic rate, survival, reproduction, migration and diffusion [21-25]. This can affect the geographical distribution of insects [26]. Previous study showed that as the global climate warmed up, pests spread from low latitudes to high latitudes and from low altitudes to high altitudes [27-29]. In addition, climatic factors tend to affect the growth of crops, resulting in changes in the phenological synchronicity of the species, which also changes the suitable distribution of insects [30]. However, there is still a gap on the potential distribution areas of RWW under future climatic conditions.

In this study, we used the RWW distribution data issued by the Ministry of Agriculture and Rural Affairs in the People's Republic of China in 2021 and optimized the MaxEnt model for forecasting the potential distribution areas of RWW under the current and future scenarios of SSP126 (belonging to the low forcing scenario, where the radiative forcing will stabilize at approximately 2.6 W/m^2 in 2100), SSP245 (belonging to the moderate radiative forcing scenario, where the radiative forcing will stabilize at approximately 4.5 W/m^2 in 2100) and SSP585 (belonging to the high forcing scenario, where the radiative forcing will reach 8.5 W/m^2 by 2100) in the 2030s, 2050s, 2070s and 2090s [31]. This study will provide a reference for the monitoring, early warning and effective prevention and control of RWW.

Experimental

Data Sources and Processing

Basic geographic data were downloaded from the National Geomatics Center of China (<http://ngcc.sbsm.gov.cn/>).

Host distribution data: Following the research by Liu et al. [32] on the results of rice cropping regions in China, we used ArcGIS10.4 (<https://www.esri.com/>) to extract the distribution data of rice in China (Fig. 1).

Species Occurrence Data: According to The National Agricultural Plant Quarantine Pests Administrative Region List issued by the Ministry of Agriculture and Rural Affairs of the People's Republic of China in 2021, RWW was distributed in 450 counties in 25 provinces in China. The occurrence points were extracted by the Baidu coordinate picking system (<http://api.map.baidu.com/lbsapi/getpoint/index.html>), and 450 occurrence points of RWW were obtained. To avoid the overfitting of occurrence points that influence the model predicted results, we used ENMTools v1.3 (<http://purl.oclc.org/enmtools>) software to filter species occurrence points. ENMTools sampled from grid files and filtered points in each grid cell so that only 1 suitable point was retained [33]. After filtering, 444 occurrence points remained (Fig. 2).

Environmental Data: The environmental data were downloaded from the WorldClim data website (WorldClim, <https://www.worldclim.org/>). We selected WorldClim 2.1 climate data for research. The current environmental data included 19 environmental variables from 1970 to 2000. Future environmental data covered 19 environmental variables in the 2030s (2021-2040), 2050s (2041-2060), 2070s (2061-2080), and 2090s (2081-2100) under the SSP126, SSP245 and SSP585 scenarios in the BBC-CSM2-MR climate model [34]. The spatial resolution of the environmental data was 2.5 min. Nineteen environmental variables and RWW occurrence



Fig. 1. The distribution of rice cropping regions in China. Based on Liu et al. [30]; ArcGIS10.4 was used to extract the distribution data of rice in China.

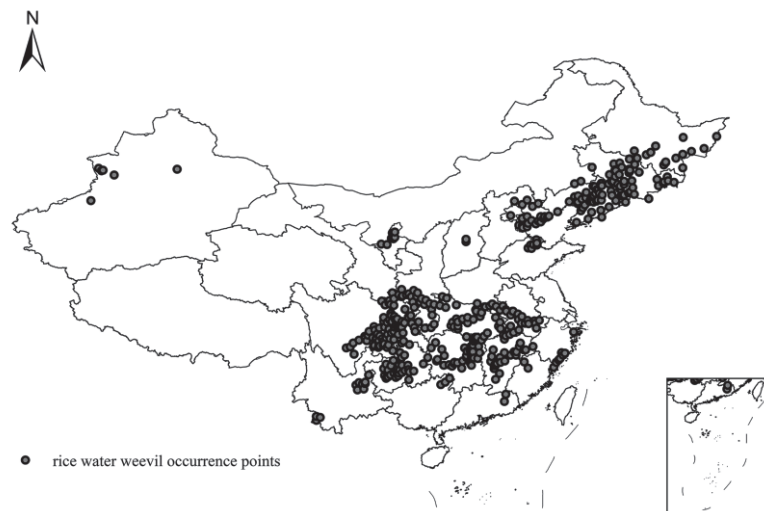


Fig. 2. The RWW occurrence points in China after filtering by ENMTools to avoid the overfitting of occurrence points that influence the predicted results. 444 occurrence points remained.

data after filtering were imported into the MaxEnt model (version 3.4.1, http://biodiversityinformatics.amnh.org/open_source/maxent) for modeling and analysis. First, variables with contribution scores <5% in MaxEnt were discarded. Then, ENMTools was used for correlation analysis of environmental variables. Finally, with the contribution rate as the standard, the variables with a low contribution rate among the variables with a Pearson correlation value ≥ 0.7 were deleted.

MaxEnt Model Optimization

Based on the filtered species occurrence data and environmental variables, the ENMeval (Version 0.3.1, <https://CRAN.R-project.org/package=ENMeval>) packet

was run in R 3.6.3 to optimize the regularization multiplier (RM) and feature combination (FC) parameters which were closely related to the complexity of MaxEnt model. MaxEnt has 5 FC: linear-L, quadratic-Q, hinge-H, product-P and threshold-T [35]. Appropriate RM and FC parameters can improve the performance of MaxEnt to avoid overfitting of the model predicted results [36]. The Akaike information criterion (AIC) is a standard method to measure statistical model fitting [37]. AIC gives priority to the model with the lowest AICc value [38]. In this study, RM was set to 0.5, 1.0, 1.5, 2.0, 2.5, 3.0, 3.5 and 4.0, and FC included 6 combinations of L, LQ, H, LQH, LQHP and LQHPT [39, 40]. Finally, the combination of RM and FC with a delta AICc value < 2 or $= 0$ was selected as the Maxent model parameters [41].

Potentially Suitable Areas

The filtered RWW occurrence data, environmental variables and parameters of RM and FC were imported into MaxEnt model. The random test percentage was set to 25, indicating that 75% of the occurrence points were randomly selected as the training set, while the remaining 25% were used as the test set. This process was repeated 10 times. The suitable areas in the current period and the 2030s, 2050s, 2070s, and 2090s under the SSP126, SSP245, and SSP585 scenarios were predicted. The receiver operating characteristic (ROC) curve and the AUC value were used to evaluate the MaxEnt model. For the AUC value range from 0.5 to 1, the output showing $0.5 \leq \text{AUC} \leq 0.6$ was considered to have no predictive ability; $0.6 < \text{AUC} \leq 0.7$ had a poor predictive ability; $0.7 < \text{AUC} \leq 0.8$ had a general predictive ability; $0.8 < \text{AUC} \leq 0.9$ had a moderate predictive ability; and $0.9 < \text{AUC} \leq 1.0$ had a high predictive ability [42]. The jackknife test was used to assess the relative importance of different environmental variables. According to the response of species distribution probability to environmental variables, we analyzed the suitability thresholds of major environmental variables that controlled the potential distribution of species. The *.asc format file resulting from the MaxEnt model was imported into ArcGIS10.4 for mask extraction and reclassification. The 10th percentile training presence logistic threshold was selected as the threshold value to define the existence of species [42]. Finally, four classes of suitability were determined as follows: unsuitable area ($P < 0.43$), low suitable area ($0.43 \leq P < 0.54$), moderately suitable area ($0.54 \leq P < 0.67$), and highly suitable area ($P \geq 0.67$).

Analysis of Centroid Migration

The *.asc format files of current and future climate conditions were imported into ArcGIS10.4. SDMtoolbox (Version 2.4, <http://www.sdmttoolbox.org/downloads>) which was loaded into ArcGIS10.4 for analyzing the centroid migration between the current and future climatic conditions. The computational geometry in ArcGIS10.4 was used to find the coordinates of the centroids. The distance between two centroids was calculated by proximity analysis in ArcGIS10.4.

Results and Discussion

MaxEnt Model Optimization Results

The regularization multiplier (RM) and feature combination (FC) in the Maxent model were optimized based on the ENMeval package in R. The results showed that the parameters that confirmed delta $\text{AICc} = 0$ were $\text{RM} = 1.5$, $\text{FC} = \text{LQ}$ (linear and quadratic), and $\text{RM} = 4$, $\text{FC} = \text{LQ}$ (linear and quadratic) (Fig. 3). When $\text{RM} = 1.5$, the AUC value was 0.9765, and when $\text{RM} = 4$, the AUC value was 0.9809. The higher the AUC value was, the better the accuracy of the model prediction. Therefore, the model parameters $\text{RM} = 4$ and $\text{FC} = \text{LQ}$ were used for simulating the potential distribution of RWW.

Model Evaluation Results

ROC curves were used to test the accuracy of the predicted suitable area of RWW by MaxEnt model.

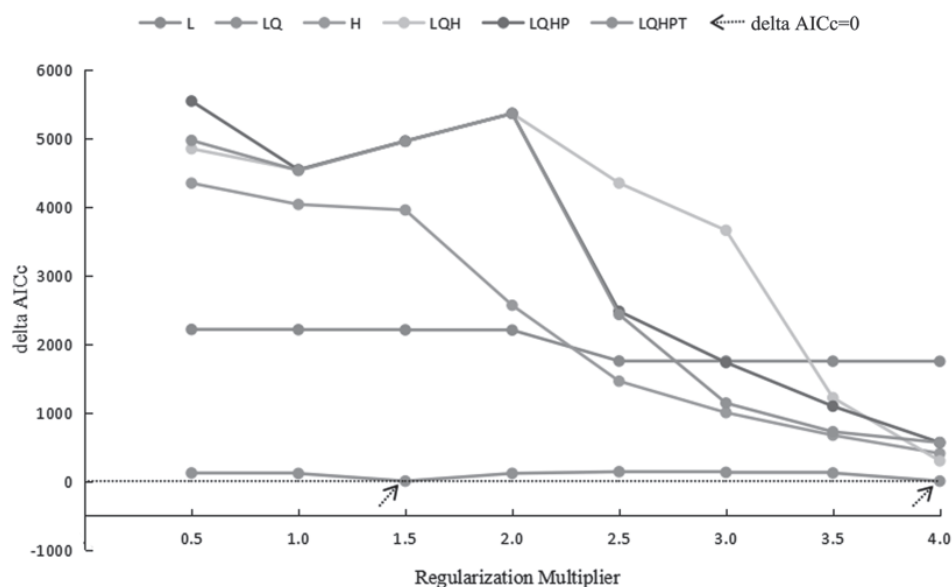


Fig. 3. The regularization multiplier (RM, set to 0.5, 1.0, 1.5, 2.0, 2.5, 3.0, 3.5 and 4.0) and feature classes (FC, included 6 combinations of L, LQ, H, LQH, LQHP and LQHPT) of RWW in the Maxent model. The black dashed arrow indicates $\text{delta AICc} = 0$, at this time, $\text{RM} = 1.5$, $\text{FC} = \text{LQ}$ and $\text{RM} = 4$, $\text{FC} = \text{LQ}$.

Table 1. The AUC value simulated by the MaxEnt model under different climate scenarios.

Climate Scenarios	AUC
Near current	0.968
2021-2040 SSP126	0.969
2041-2060 SSP126	0.973
2061-2080 SSP126	0.976
2081-2100 SSP126	0.975
2021-2040 SSP245	0.975
2041-2060 SSP245	0.974
2061-2080 SSP245	0.973
2081-2100 SSP245	0.973
2021-2040 SSP585	0.975
2041-2060 SSP585	0.976
2061-2080 SSP585	0.974
2081-2100 SSP585	0.975

After 10 simulations, the AUC value was 0.968 under the current climatic conditions, and these AUC values ranged from 0.969 to 0.976 under the future climatic conditions; all were greater than 0.9 (Table 1). According to the evaluation criteria of the ROC curve, the accuracy of prediction were “very good”, and the predicted distribution of the model fit well with the actual distribution of species.

Importance Analysis of Environmental Variables

The contribution rate and Pearson correlation analysis were used to select environmental variables. The contribution rate of precipitation of the warmest quarter (Bio18) was highest, accounting for 56.9%, followed by temperature seasonality (Bio4), mean temperature of the coldest quarter (Bio11) and precipitation seasonality (Bio15), accounting for 16.2%, 6.8% and 5.8%, respectively (Table 2). The importance

Table 2. Percent contribution and permutation importance of environmental variables to model simulations. Bio4: temperature seasonality; Bio11: mean temperature of the coldest quarter; Bio15: precipitation seasonality; Bio18: precipitation of the warmest quarter.

Variable	Percent contribution (%)	Permutation importance
Bio18	56.9	10.9
Bio4	16.2	0.7
Bio15	6.8	1.8
Bio11	5.8	13.3

of 4 environmental variables following 10 repetitions was shown in the jackknife test figure (Fig. 4). The longer the blue bar is, the more influential the variable is on the species distribution, and the shorter the green bar is, the more information the variable has compared to others. The maximum gain was obtained when Bio11 was used alone, followed by Bio18, Bio15, and Bio4. The gain was minimal when Bio4 was used alone. When Bio11 was removed, the reduced gain was maximum, followed by Bio18. Therefore, Bio11 and Bio18, which contained more information than the other variables, were the dominant environmental variables effected the distribution of RWW.

The response curves between the dominant environmental variables Bio4, Bio11, Bio15, and Bio18 and the distribution probability were drawn (Fig. 5). The results indicated that the suitable range of temperature seasonality (Bio4) was 652~1308. The optimum range for the mean temperature of the coldest quarter (Bio11) was -9.1~9.2°C. When the temperature was -9.1~1.3°C, the distribution probability increased with increasing temperature. When the temperature was 1.3~9.2°C, the distribution probability decreased with increasing temperature. The suitable range of precipitation seasonality (Bio15) was 58~123. When the coefficient was 58~99, the distribution probability increased with the increasing coefficient. Afterward, the coefficient continued to increase, the change was more drastic, and the distribution probability decreased. The suitable range of precipitation of the warmest quarter (Bio18) was 404~3534 mm. When the precipitation of the warmest quarter was 404~3147 mm, the distribution probability increased with increasing precipitation. When the precipitation was 3147~3534 mm, the distribution probability of RWW decreased with increasing precipitation, and the reduction was large.

Potential Distribution of RWW under the Current Climatic Conditions.

The total suitable area of RWW in China was 391.0698 million hm², accounting for 40.77% of China's total area (Fig. 6, Table 3). The suitable areas were mainly distributed in east China, central China and south China, with a few distributions in other regions. Unsuitable areas, low suitable areas, moderately suitable areas and highly suitable areas accounted for 59.23%, 18.29%, 14.01% and 8.47% of China's total area, respectively. The highly suitable areas were mainly distributed in Shandong, Liaoning, Hebei and Anhui Province. Shandong Province covered the largest highly suitable areas, accounting for 18.83%. Liaoning Province and Hebei Province accounted for 14.87% and 13.52%, respectively. The moderately suitable areas were mainly distributed in Hubei, Guangxi Zhuang Autonomous Region, Sichuan and Zhejiang Province. Among them, Hubei Province had the largest moderately suitable area, accounting for 10.69%. The Guangxi Zhuang Autonomous Region and

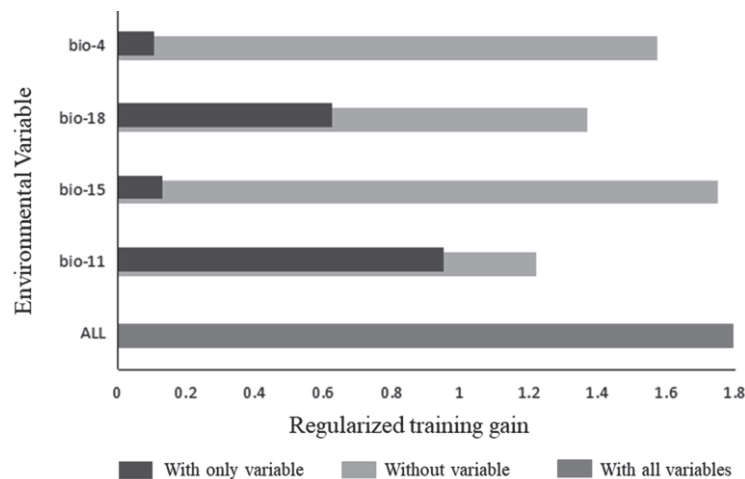


Fig. 4. Jackknife analytical results showed the most influential environmental variables predicting potentially suitable distribution areas of RWW in China. Blue bar represents the regularized training gain for models using a single variable only; Green bar represents the jackknife without that single variable; Red bar represents the jackknife with all variables.

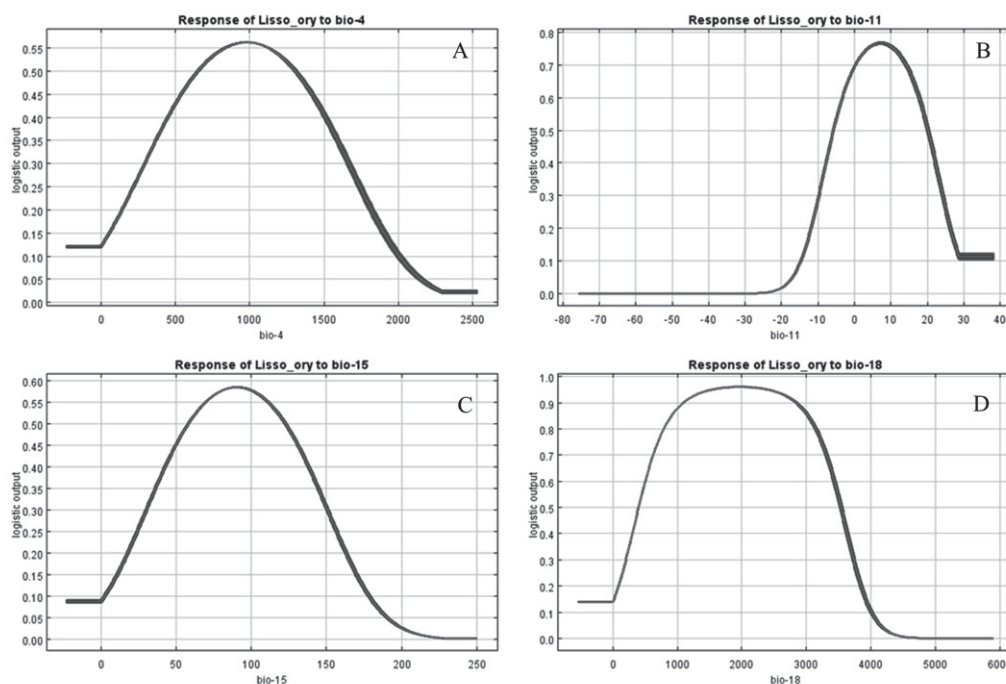


Fig. 5. Response curves between the distribution probability of RWW and environmental variables. a) temperature seasonality (Bio4), b) mean temperature of the coldest quarter (Bio11), c) precipitation seasonality (Bio15), d) precipitation of the warmest quarter (Bio18). Blue margins show \pm SD calculated over 10 replicates.

Sichuan Province accounted for 9.43% and 8.37%, respectively. The low suitable areas were mainly distributed in Xinjiang Uygur Autonomous Region, Inner Mongolia Autonomous Region, Guizhou, Guangdong and Shannxi Province. Among them, Xinjiang Uygur Autonomous Region had the largest area of low suitability, accounting for 22.12% of the total area of low suitability. The second was the Inner Mongolia Autonomous Region, accounting for 12.83%. The unsuitable areas were mainly distributed in the

Xinjiang Uygur Autonomous Region, Tibet Autonomous Region, Inner Mongolia Autonomous Region, Qinghai, Gansu, Yunnan and Heilongjiang Province. The Xinjiang Uygur Autonomous Region had the largest unsuitable areas, followed by the Tibet Autonomous Region and Inner Mongolia Autonomous Region, which accounted for 21.22%, 20.24% and 15.36% of the total area of unsuitable areas, respectively.

The RWW distribution area had a high degree of overlap with rice cropping regions in China.

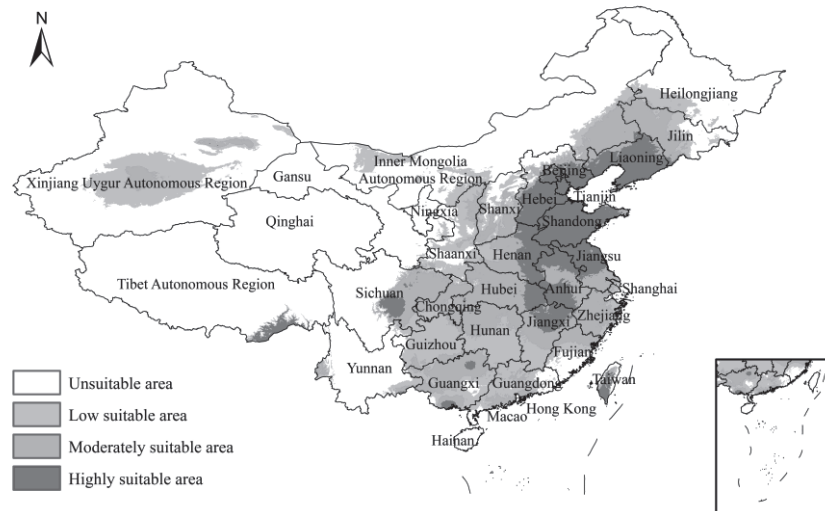


Fig. 6. The potential distribution area of RWW in China under current climatic conditions.

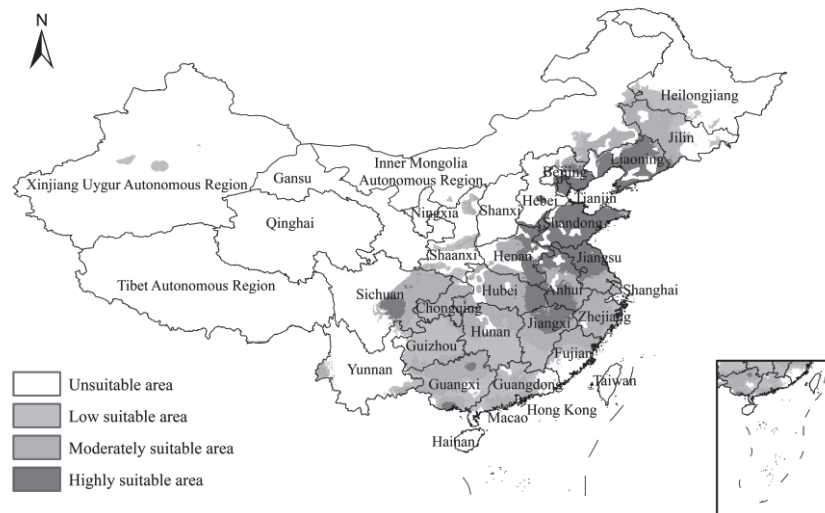


Fig. 7. The potential distribution area of RWW in China based on a comprehensive analysis of the predicted results of the model under current climatic conditions and rice-cropping regions. non-growing regions were classified as unsuitable areas for RWW.

The suitable areas of RWW were mainly distributed in southern China double cropping rice region, central China double single cropping rice region and eastern China cropping rice region. The highly suitable areas were mainly distributed in the central and eastern China rice regions (Fig. 7).

Potential Distribution of RWW under Future Climatic Conditions

The suitable area of RWW would increase, and the highly suitable area would increase the most, while the low suitable area and moderately suitable areas would decrease under different scenarios and periods in the future (Figs 8, 9, Table 4).

Under the SSP126 scenario, from the present to the 2090s, the change in the unsuitable area showed a

trend of decreasing first and then increasing. Compared with the current values, the unsuitable area would decrease by 9.74% (2030s) and increased by 11.14% (2050s), 7.59% (2070s), and 7.61% (2090s). The change in the low suitable area showed a decreasing trend, and the decreasing range gradually increased. The area would decrease by 11.58% (2030s), 37.62% (2050s), 55.92% (2070s) and 54.28% (2090s). The change in the moderately suitable area would first increase and then decrease. It would increase by 27.77% (2030s) and decrease by 15.71% (2050s), 10.86% (2070s), and 7.12% (2090s). The change in the highly suitable area would increase gradually. It would increase by 47.23% (2030s), 29.35% (2050s), 85.75% (2070s) and 75.81% (2090s).

Under the SSP245 scenario, from the present to the 2090s, the unsuitable area of RWW showed an overall trend of first increasing and then decreasing.

Table 3. Prediction of the areas (ten thousand hm²) and proportion (%) of different suitable areas of RWW in China under current climatic conditions.

Provinces (autonomous regions and municipalities)	Unsuitable area		Low suitable area		Moderately suitable area		Highly suitable area	
	Area (ten thousand hm ²)	Proportion of unsuitable area (%)	Area (ten thousand hm ²)	Proportion of low suitable area (%)	Area (ten thousand hm ²)	Proportion of moderately suitable area (%)	Area (ten thousand hm ²)	Proportion of highly suitable area (%)
Beijing	0.16	0.00	3.93	0.02	30.93	0.23	129.10	1.59
Tianjin	0.00	0.00	0.00	0.00	0.17	0.00	118.86	1.46
Hebei Province	296.44	0.52	234.98	1.34	242.72	1.81	1097.45	13.52
Shanxi Province	279.79	0.49	709.20	4.04	577.31	4.30	0.68	0.01
Inner Mongolia Autonomous Region	8726.43	15.36	2251.72	12.83	954.17	7.10	28.82	0.36
Liaoning province	0.00	0.00	0.33	0.00	273.56	2.04	1206.95	14.87
Jilin Province	407.14	0.72	547.68	3.12	917.20	6.83	30.31	0.37
Heilongjiang Province	3549.08	6.25	823.54	4.69	24.40	0.18	0.00	0.00
Shanghai	0.63	0.00	38.38	0.22	24.38	0.18	0.00	0.00
Jiangsu Province	0.00	0.00	8.54	0.05	351.49	2.62	663.75	8.18
Zhejiang Province	7.17	0.01	203.63	1.16	812.43	6.05	11.70	0.14
Anhui Province	0.00	0.00	0.00	0.00	504.21	3.75	891.94	10.99
Fujian Province	432.26	0.76	427.95	2.44	368.49	2.74	0.00	0.00
Jiangxi Province	0.00	0.00	470.41	2.68	673.42	5.01	526.81	6.49
Shandong Province	0.00	0.00	0.00	0.00	53.24	0.40	1528.95	18.83
Henan Province	0.72	0.00	201.43	1.15	678.63	5.05	787.07	9.69
Hubei Province	0.55	0.00	104.49	0.60	1436.40	10.69	316.05	3.89
Hunan Province	0.00	0.00	1113.91	6.35	997.22	7.42	7.20	0.09
Guangdong Province	286.05	0.50	1179.14	6.72	277.27	2.06	0.00	0.00
Guangxi Zhuang Autonomous Region	73.69	0.13	921.18	5.25	1267.19	9.43	112.31	1.38
Hainan Province	309.70	0.55	0.00	0.00	0.00	0.00	0.00	0.00
Chongqing	1.85	0.00	237.54	1.35	584.31	4.35	0.00	0.00

Table 3. Continued.

Sichuan Province	3117.17	5.49	396.83	2.26	1123.88	8.37	279.28	3.44
Guizhou Province	86.54	0.15	1433.40	8.17	241.67	1.80	0.00	0.00
Yunnan Province	3321.69	5.85	478.58	2.73	134.43	1.00	5.59	0.07
Tibet Autonomous Region	11501.22	20.24	99.29	0.57	97.83	0.73	242.13	2.98
Shaanxi Province	424.81	0.75	1370.51	7.81	260.97	1.94	0.00	0.00
Gansu Province	4295.66	7.56	252.56	1.44	0.36	0.00	0.00	0.00
Qinghai Province	6966.10	12.26	0.00	0.00	0.00	0.00	0.00	0.00
Ningxia Hui Autonomous Region	568.71	1.00	95.29	0.54	0.00	0.00	0.00	0.00
Xinjiang Uygur Autonomous Region	12058.90	21.22	3883.27	22.12	457.34	3.40	0.65	0.01
Hong Kong Special Administrative Region	0.00	0.00	3.68	0.02	7.36	0.05	0.00	0.00
Macao Special Administrative Region	0.00	0.00	0.00	0.00	0.29	0.00	0.00	0.00
Taiwan Province	105.26	0.19	61.54	0.35	62.14	0.46	132.99	1.64
Total area	56817.73	100.00	17552.92	100.00	13435.44	100.00	8118.62	100.00

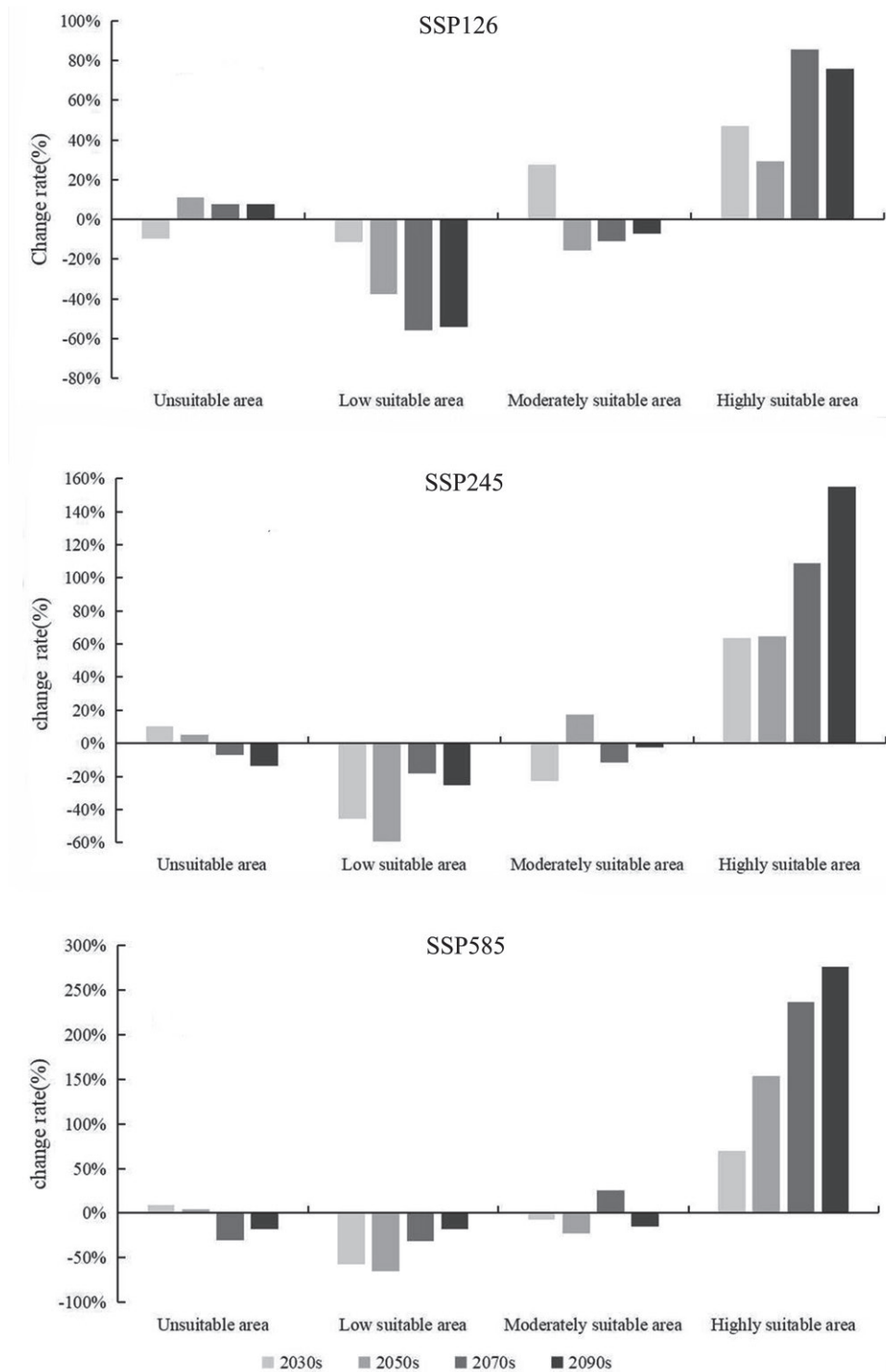


Fig. 8. Changes of unsuitable area, low suitable area, moderately suitable area and highly suitable area of RWW under three different climate scenarios (SSP126, SSP245, and SSP585) in the 2030s, 2050s, 2070s and 2090s.

Compared with the current values, the increases would be 10.44% (2030s) and 5.08% (2050s), and the decreases would be 7.22% (2070s) and 13.7% (2090s). The low suitable area showed a decreasing trend, decreasing by 45.71% (2030s), 59.47% (2050s), 18.06% (2070s) and 25.35% (2090s). The moderately suitable area would first decrease, then increase and finally decrease,

decreasing by 22.94% (2030s), increasing by 17.12% (2050s), and decreasing by 11.46% (2070s) and 2.48% (2090s), respectively. The change in the highly suitable area showed an increasing trend over a large range. Compared with the current area, the highly suitable area would increase by 63.74% (2030s), 64.69% (2050s), 108.55% (2070s) and 154.79% (2090s).

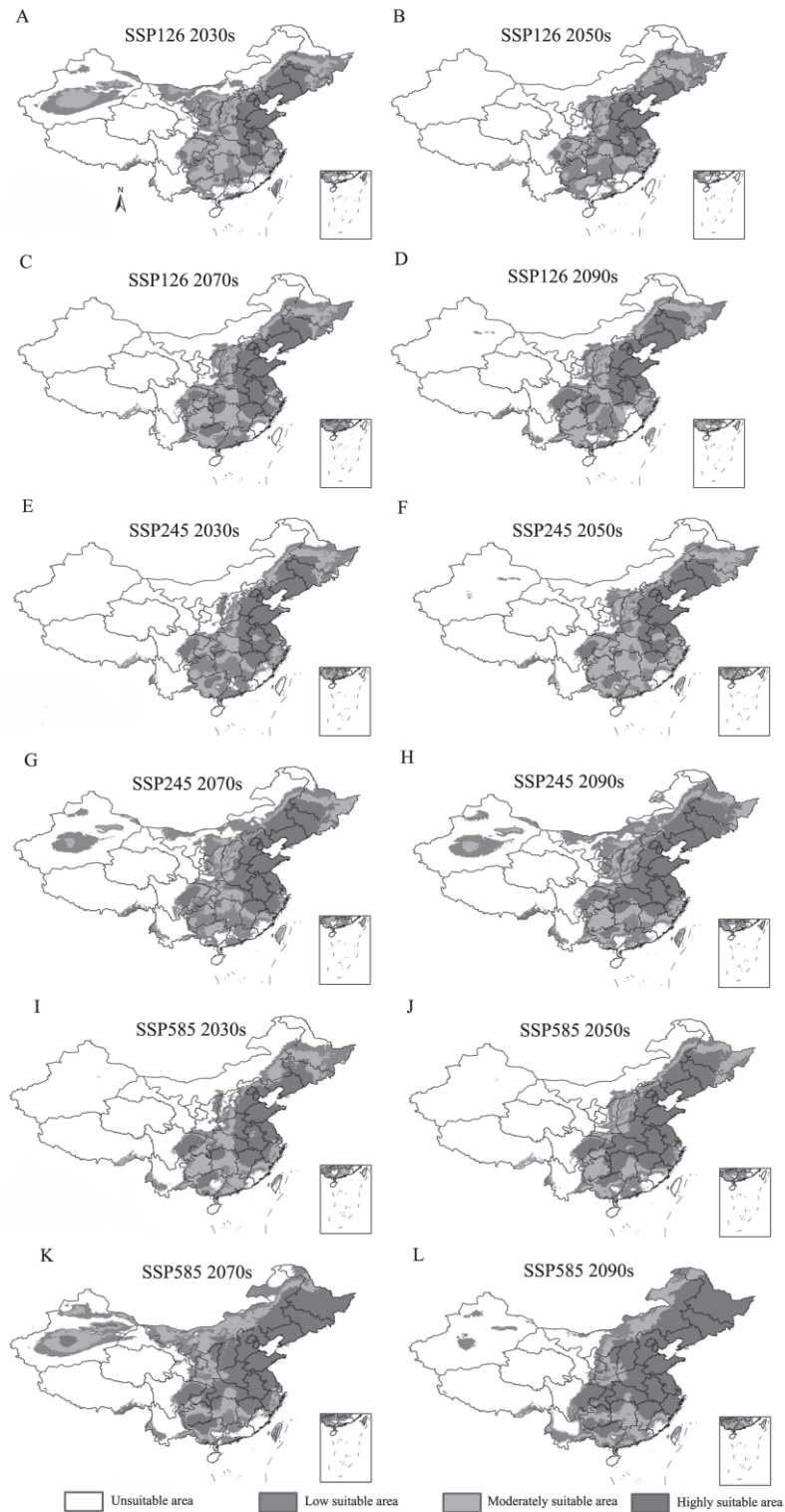


Fig. 9. The future potential distribution of RWW under the SSP126, SSP245, and SSP585 climate scenarios by 2030s, 2050s, 2070s and 2090s. A:SSP126-2030s; B: SSP126-2050s; C: SSP126-2070s; D: SSP126-2090s; E: SSP245-2030s; F:SSP245-2050s; G:SSP245-2070s; H: SSP245-2090s; I: SSP585-2030s; J: SSP585-2050s; K: SSP585-2070s; L: SSP585-2090s.

Under the SSP585 scenario, from the present to the 2090s, the unsuitable area of RWW would first increase and then decrease, increasing by 9.47% (2030s) and 3.87% (2050s) and decreasing by 30.04% (2070s) and 17.53% (2090s). The low suitable area would decrease,

decreasing by 57.57% (2030s), 65.61% (2050s), 31.37% (2070s) and 17.53% (2090s). The moderately suitable area would first decrease, then increase and finally decrease. Compared with the current situation, the area would decrease by 7.22% (2030s) and 23.25% (2050s),

Table 4. Prediction of the area (ten thousand hm²) and rate of change (%) of different RWW suitable areas in China under future climate conditions.

Climate Scenarios		Unsuitable area		Low suitable area		Moderately suitable area		Highly suitable area	
		Area (ten thousand hm ²)	Rate of change (%)	Area (ten thousand hm ²)	Rate of change (%)	Area (ten thousand hm ²)	Rate of change (%)	Area (ten thousand hm ²)	Rate of change (%)
Current		56817.73		17552.92		13435.44		8118.62	
SSP126	2030s	51284.61	-9.74	15519.89	-11.58	17167.09	27.77	11953.12	47.23
	2050s	63148.27	11.14	10949.47	-37.62	11325.32	-15.71	10501.64	29.35
	2070s	61131.45	7.59	7736.76	-55.92	11976.49	-10.86	15080.01	85.75
	2090s	61146.85	7.61	8025.57	-54.28	12478.83	-7.12	14273.46	75.81
SSP245	2030s	62750.1	10.44	9528.62	-45.71	10352.82	-22.94	13293.17	63.74
	2050s	59705.06	5.08	7113.63	-59.47	15735.15	17.12	13370.87	64.69
	2070s	52714.64	-7.22	14382.65	-18.06	11896.37	-11.46	16931.06	108.55
	2090s	49033.32	-13.70	13103.34	-25.35	13102.65	-2.48	20685.4	154.79
SSP585	2030s	62199.3	9.47	7448.47	-57.57	12464.9	-7.22	13811.95	70.13
	2050s	59017.56	3.87	6035.74	-65.61	10311.64	-23.25	20599.77	153.73
	2070s	39749.73	-30.04	11982.54	-31.73	16886.58	25.69	27305.85	236.34
	2090s	46859.03	-17.53	7162.08	-17.53	11381.74	-15.29	30521.86	275.95

increase by 25.69% (2070s) and decrease by 15.29% (2090s). The highly suitable area showed an increasing trend with a large range, increasing by 70.13% (2030s), 153.73% (2050s), 236.34% (2070s) and 275.95% (2090s).

The unsuitable area would decrease the most under the SSP585 scenario in the 2070s and 2090s and would increase the most under the SSP126 scenario in the 2050s and SSP245 scenario in the 2030s. Under the SSP585 scenario in the 2030s and 2050s and the SSP245 scenario in the 2050s, the low suitable area would decrease the most. The moderately suitable area would decrease the most under the SSP245 scenario in the 2030s and the SSP585 scenario in the 2050s and would increase the most under the SSP126 scenario in the 2030s. The highly suitable area would increase the most under the SSP585 scenario in the 2070s and 2090s.

Centroid Migration of RWW in Suitable Areas under Future Climatic Conditions

According to Fig. 10 and Table 5, the centroid of RWW in China was located in Henan Province under current climatic conditions.

Under the SSP126 scenario, the centroid of the RWW suitable area would migrate northwestward to the southern of Shanxi Province by the 2030s. By the 2050s, it would continually move southeastward. By the 2070s, the centroid of RWW would move southwestward. From the 2070s to the 2090s, it would migrate northwestward to the southern of Shandong Province.

Under the SSP245 scenario, the centroid would migrate northeastward from Henan to southern Shandong by the 2030s. From the 2050s to the 2070s, the centroid would move southwestward, then northwestward. By the 2090s, the centroid would migrate to the northern of Henan Province.

Under the SSP585 scenario, from the present to the 2050s, the centroid would migrate southeastward to Shandong Province. By the 2070s, the centroid would migrate northwestward. By the 2090s, it would migrate southeastward to the Shandong Province.

Comparing the current and 2090s, the centroid of RWW suitable area would migrate eastward and northward in all three scenarios.

Discussion

As an agricultural pest, RWW poses a threat to China's agricultural production, especially to rice [43]. RWW has continued to spread in China. Climate change broadens the suitable areas of insects and promotes the invasion and colonization of insects to other regions [44, 45]. At the same time, climate change also affects the suitable areas of plants, and changes in host plant distribution can also have a certain impact on the distribution of insects [46, 47]. There is a gap in the research on the suitable area of RWW under future climatic conditions. Therefore, it is of great significance to explore the effects of climate change on the distribution of RWW and to formulate quarantine measures for monitoring and warning of RWW.

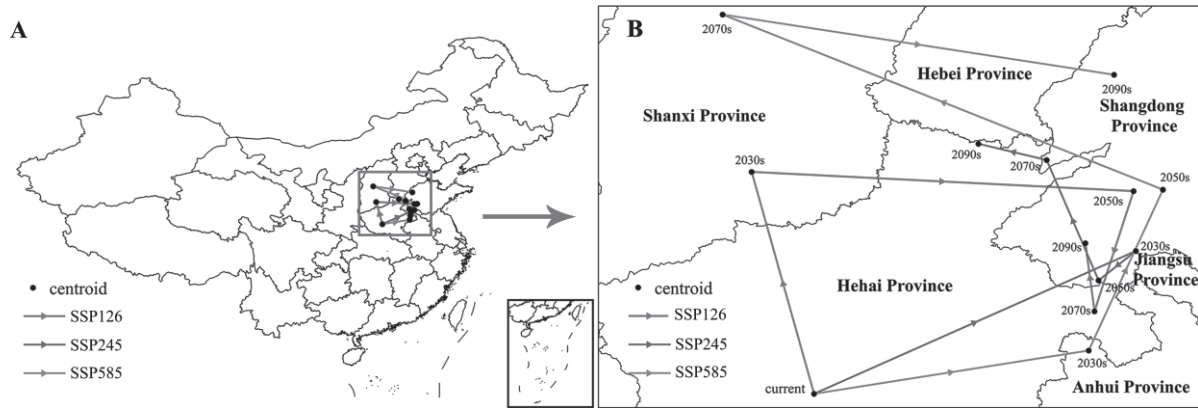


Fig. 10. Centroid movement of RWW under the SSP126, SSP245, and SSP585 climate scenarios by 2030s, 2050s, 2070s and 2090s. Climate scenarios were distinguished by different color line: the SSP126 was displayed by a red line, SSP245 was displayed by a blue line and SSP585 was displayed by a green line. a) Movement of the centroid of RWW in China; b) Enlarged view of the red box in A.

Table 5. Shift centroid coordinates, distance and direction of the Centroids of RWW under different future climatic conditions.

Climate Scenarios	Period	Centroid Coordinates		Direction	Displacement (km)
		Longitude (°E)	Latitude (°N)		
	Current	112.9027	33.4177		
SSP126	2030s	112.2306	35.8039	Northwest	25.98
	2050s	116.3453	35.5967	Southeast	39.76
	2070s	115.9244	34.3046	Southwest	14.16
	2090s	115.8261	35.0372	Northwest	7.78
SSP245	2030s	116.3700	34.9535	Northeast	37.20
	2050s	115.9678	34.6373	Southwest	5.11
	2070s	115.4090	35.9309	Northwest	14.57
	2090s	114.6736	36.1056	Northwest	7.32
SSP585	2030s	115.8617	33.8838	Southeast	28.98
	2050s	116.6615	35.6125	Southeast	19.77
	2070s	111.9170	37.4954	Northwest	49.71
	2090s	116.1352	36.8480	Southeast	41.23

MaxEnt, CLIMEX and ArcView were used to study the suitable areas of RWW [12, 19, 20]. The MaxEnt model can complete the simulation analysis of the suitable area of RWW under current and future climatic conditions, and the prediction results are stable, reliable, and easy to interpret. It has been widely applied to various species [48,49]. However, the default parameters of the MaxEnt model were predominantly used in previous studies, which could lead to excessive model fitting [50, 51]. To solve this problem, adjusted RM and FC parameters in the MaxEnt model would reduce the complexity and model overfitting in the species distribution [52, 53]. This study used the ENMeval packet based on R developed by Muscarella et al. [36] to optimize the MaxEnt model parameters. We evaluated the complexity of the MaxEnt model by using

AIC values (AICc) and selected a combination of delta AICc = 0 to improve the prediction ability of MaxEnt and reduce the influence of the overfitting of the model to species distribution points [54].

In this study, the optimized MaxEnt model and ENMTools were used to conduct correlation analysis and jackknife tests on 19 bioclimatic variables. The results showed that the temperature seasonality (Bio4), mean temperature of the coldest quarter (Bio11), precipitation seasonality (Bio15), and precipitation of the warmest quarter (Bio18) were most closely related to the RWW distribution. Li et al. [55] showed that the occurrence period of RWW was closely related to the annual temperature change. The temperature change from April to May affects the occurrence period of overwintering adults and first-generation

larvae. In the second half of April, RWW begin to migrate into the early rice field. The time of peak migration is also correlated with temperature [56], and precipitation affects air temperature, especially during April and May. Rain leads to low temperatures, which delay the occurrence of overwintering adults and the main migration peak. In contrast, low rainfall and high temperature lead to an earlier occurrence of overwintering adults and the main migration peak. In this study, precipitation of the warmest quarter (Bio18), <404 mm or >3534 mm, was not suitable for the survival of RWW. Therefore, too little or too much precipitation influences air temperature, which then affects the growth and development of RWW and their migration time, thus affecting their distribution area.

Rice is the main host plant of RWW, and its distribution has a specific influence on the distribution of RWW [57]. Rice cropping regions are mainly distributed in central China, south China, east China and northeast China, with sporadic planting in northwest China [58, 59]. This result suggested that there was considerable overlap between the suitable area of RWW and rice cropping regions in China. Our results were approximately the same as Qi et al. [12]. However, the distributions of low, moderately and highly suitable areas were different. These differences may be attributed to the different environmental variables and model parameters of MaxEnt.

In this study, the total suitable area of RWW under future climatic conditions would increase, showing a trend of eastward and northward migration. The highly suitable area would increase most significantly, and the trend of northern expansion would be obvious. However, the moderately suitable areas would show a decreasing trend overall. The diffusion of the moderately suitable area would mainly occur in south China. The decreasing trend of the low suitable area would be more obvious than that of the moderately suitable area, and the low suitable area would mainly change into the moderately suitable area and the highly suitable area in the future. The analysis of the centroid migration of RWW showed that the centroid could migrate to the east and north in the future, though the northern trend would be more obvious. The centroid would migrate from Henan Province to Anhui, Shandong, Hebei and Shanxi Province. The potential planting boundary of single- and double-cropping rice in China would move significantly northward due to climatic warming [60], and the suitable distribution area of RWW would also moving northward. Therefore, the RWW may cause economic losses due to its widespread northern trend.

In conclusion, the management of RWW invasion should be strengthened in rice cropping regions. Physical, chemical and biological control measures should be adopted to contain any increased risk. Quarantine measures should be strengthened, and strict management measures should be formulated to prevent the invasion of RWW into rice cropping regions

without the occurrence of this pest. The predicted results of suitable areas in the future can provide a reference for the monitoring and prevention of RWW, timely adjustment of key prevention and control areas based on field investigation, and formulation of targeted quarantine measures.

Conclusions

The results of this study revealed the suitable distribution of the RWW in China under current and future climatic conditions. Under the current climatic conditions, the suitable areas mainly included eastern China, central China and southern China and covered 391.0698 million hm², accounting for 40.77% of China. There was considerable overlap between the suitable areas of RWW and rice cropping in China. Under future climatic conditions, the suitable areas of RWW would increase. Among them, the highly suitable areas of would increase significantly under SSP126, SSP245 and SSP585. The centroid migration in the suitable areas of RWW showed a trend of moving eastward and northward. The results of this study can provide theory and data support for early warning and quarantine inspection.

Acknowledgments

This work was supported by Science and Technology Plan Projects in Sichuan Province, China [2021YFYZ0021], Modern Agricultural Industry Technology System of Sichuan Innovation Team [SCCXTD-2020-04] and the Technological Development of Meteorological Administration/Heavy Rain and Drought Flood Disasters in Plateau and Basin Key Laboratory of Sichuan Province, China [Key Laboratory of Sichuan Province-2018-Key-05-11].

Conflict of Interest

The authors declare no conflicts of interest.

References

1. TINDALL K.V., STOUT M.J. Use of common weeds of rice as hosts for the rice water weevil (Coleoptera: Curculionidae). *Environmental Entomology*, **32**, 1227, **2003**.
2. WAN F.H., YANG N.W. Invasion and Management of Agricultural Alien Insects in China. *Annual Review of Entomology*, **61**, 77, **2016**.
3. STOUT M.J., RICE W.C., RING D.R. The influence of plant age on tolerance of rice to injury by the rice water weevil, *Lissorhoptrus oryzophilus* (Coleoptera: Curculionidae). *Bulletin of Entomological Research*, **92**, 177, **2002**.

4. ZOU L., STOUT M.J., DUNAND R.T. The effects of feeding by the rice water weevil, *Lissorhoptrus oryzophilus* Kuschel, on the growth and yield components of rice, *Oryza sativa*. *Agricultural and Forest Entomology*, **6**, 47, **2004**.
5. STOUT M.J., HAMM J.C., ABBE I., BERGERON C. The influence of rice plant age on susceptibility to the rice water weevil, *Lissorhoptrus oryzophilus*. *Journal of Applied Entomology*, **137**, 241, **2013**.
6. MÁRCIO BARTZ D.N., JOSÉ FRANCISCO D.S.M., ANDERSON D.G., CRISLAINE ALVES BARCELLOS D.L., GERMANO T.B. Profundidade da amostragem de solo e de raízes e índice de infestação de *Oryzophagus oryzae* (Costa Lima, 1936) (Coleoptera: Curculionidae) em cultivares de arroz. *Ciência Rural*, **41**, 2039, **2011**.
7. AGHAEI M.A., GODFREY L.D. A century of rice water weevil (Coleoptera:Curculionidae): A history of research and management with an emphasis on the united States. *Journal of Integrated Pest Management*, **5**, D1, **2014**.
8. LUPI D., JUCKER C., ROCCO A., GIUDICI M.L., BOATTIN S., COLOMBO M. Current status of the rice water weevil *Lissorhoptrus oryzophilus* in Italy: eleven-year invasion. *EPPO Bulletin*, **45**, 123, **2015**.
9. DING X.H., LI C., WANG X.W., FU K.Y., TURSUN A., HUANG H.M., MULATI T., HE J., GUO W.C. Potential distribution and adaptability of the rice water weevil (*Lissorhoptrus oryzophilus*) in Xinjiang. *Journal of Biosafety*, **28**, 116, **2019** [In Chinese].
10. HE J., WANG X.W., GUO W.C., DING X.H., FU K.Y., ZHANG H.J. Research progress in the research on biology, ecology and integrated prevention and control techniques of rice water weevil in China. *Xinjiang Agricultural Sciences*, **57**, 2260, **2020** [In Chinese].
11. ZHANG Y.J. Occurrence characteristics and control of rice water weevil in Tanghai county. *Plant Quarantine*, **41**, **1997** [In Chinese].
12. QI G.J., GAO Y., HUANG D.C., LV L.H. Historical invasion, expansion process and the potential geographic distributions for the rice water weevil, *Lissorhoptrus oryzophilus* in China based on MAXENT. *Acta Phytophylacica Sinica*, **39**, 129, **2012** [In Chinese].
13. The National Agricultural Plant Quarantine Pests Administrative Region List. Available online: http://www.moa.gov.cn/govpublic/ZZYGLS/202104/t20210422_6366376.htm (accessed on 22 April 2021).
14. CHEN C.Q., YAO C.Y., ZHANG S.F., LIU Y.L. Forecasting of the occurrence period of rice plant weevil according to total effective temperature. *Journal of Anhui Agricultural Sciences*, **32**, 59, **2004** [In Chinese].
15. ZHANG W.J., JIANG M.X., ZHENG X.H., CHENG J.A. Measurement of cold hardiness in overwintering adults of the rice water weevil, *Lissorhoptrus oryzophilus*. *Entomological Knowledge*, 339, **2004** [In Chinese].
16. ZHANG Y.X., WANG K.X., BIN L., SHI D.Q., ZHAO R.B., WEN H., LU Z.X., LU W. Research progress on ecology of rice water weevil. *China Plant Protection*, **34**, 58, **2014** [In Chinese].
17. ZHAI B.P., CHENG J.A., HUANG E.Y., SHANG H.W., ZHENG X.H., WU J., FANG Y.J., XIA W.Q., LV X.J. Occurrence dynamics of rice water weevil in double cropping rice region of Zhejiang Province. *Scientia Agricultura Sinica*, **24**, **1997** [In Chinese].
18. Gentili R., Schaffner U., Martinoli A., Citterio S. Invasive alien species and biodiversity: impacts and management. *Biodiversity*, **22**, 1, **2021**.
19. MAO Z.N., SUN R.C., DOU X.Z., CHEN H., ZHOU M., QU G.Y., WU C.Y. Effect of low humidity and temperature on mortality of rice water weevil and its potential distribution in China. *Plant Quarantine*, **27**, **1997** [In Chinese].
20. GONG W.R., DU Y.Z., DAI L., CAI C., DIAO C.Y. Study on the suitable establishment area of rice water weevil, *Lissorhoptrus oryzophilus* (Kuschel) in China. *Journal of Yangzhou University (Agricultural and Life Science Edition)*, **28**, 79, **2007** [In Chinese].
21. J.BUNCAG M.J. Negative or Potential Impacts of Global Climate Change on Ecosystems and Biodiversity. *Journal of Innovation and Social Science Research*, **8**, 2591, **2021**.
22. KUMAR N., MILFONT T.L., KELLSTEDT P.M., ZAHARAN S., VEDLITZ A., SCHULDT J.P., KONRATH S.H., SCHWARZ N., BENJAMIN D., POR H.H., BUDESCU D., SHEPARDSON D.P., NIYOGI D., CHOI S., CHARUSOMBAT U., TOWNSEND L., KONESWARAN G., NIERENBERG D., RAMASAMY R., SWAMY A., JANG S.M., HART P.S., MISHRA A.K., SINGH V.P., JAIN S.K. A review study on global warming and climate change. *Asian Journal of Multidimensional Research*, **10**, 2278, **2021**.
23. BORKATAKI S., REDDY M.D., NANDA S.P., TAYE R.R. CLIMATE CHANGE AND ITS POSSIBLE IMPACT ON THE EXISTENCE OF INSECT PESTS. *Ecology, Environment and Conservation*, **26**, 273, **2020**.
24. KUMAR D.V.S., KRISHNAYYA P.V., RAO M.S., KUMAR P.A., RAO V.S. Impact of elevated CO₂ and temperature on growth and development of *Helicoverpa armigera* hubner. *Journal of Experimental Agriculture International*, **43**, 42, **2021**.
25. MALHI G.S., KAUR M., KAUSHIK P. Impact of Climate Change on Agriculture and Its Mitigation Strategies: A Review. *Sustainability*, **13**, 1318, **2021**.
26. SKENDŽIĆ S., ZOVKO M., ŽIVKOVIĆ I.P., LEŠIĆ V., LEMIĆ D. The Impact of Climate Change on Agricultural Insect Pests. *Insects*, **12**, 440, **2021**.
27. ZOU Y., ZHANG L.J., GE X.Z., GUO S.W., LI X., CHEN L.H., WANG T., ZONG S.X. Prediction of the Long-Term Potential Distribution of *Cryptorhynchus lapathi* (L.) under Climate Change. *Forests*, **11**, 1, **2019**.
28. DING W.C., LI H.Y., WEN J.B. Climate Change Impacts on the Potential Distribution of *Apocheima cinerarius* (Erschoff) (Lepidoptera: Geometridae). *Insects*, **13**, 59, **2022**.
29. MCCAIN C.M., GARFINKEL C.F. Climate change and elevational range shifts in insects. *Current Opinion in Insect Science*, **47**, 111, **2021**.
30. EKHOLM A., TACK A.J.M., PULKKINEN P., ROSLIN T., ZYTYNSKA S. Host plant phenology, insect outbreaks and herbivore communities-The importance of timing. *Journal of Animal Ecology*, **89**, 829, **2020**.
31. O'NEILL B.C., TEBALDI C., VAN VUUREN D.P., EYRING V., FRIEDLINGSTEIN P., HURTT G., KNUTTI R., KRIEGLER E., LAMARQUE J.F., LOWE J., MEEHL G.A., MOSS R., RIAHI K., SANDERSON B.M. The scenario model intercomparison project (ScenarioMIP) for CMIP6. *Geoscientific Model Development*, **9**, 3461, **2016**.
32. LIU Z.H., LI Z.G., TANG P.Q., LI Z.P., WU W.B., YANG P., YOU L., TANG H.J. Spatial-temporal changes of rice area and production in China during 1980-2010. *Acta Geographica Sinica*, **68**, 680, **2013** [In Chinese].
33. WARREN D.L., GLOR R.E., TURELLI M. ENMTools: a toolbox for comparative studies of environmental niche models. *Ecography*, **33**, 607, **2010**.

34. WU T.W., LU Y.X., FANG Y.J., XIN X.G., LI L., LI W.P., JIE W.H., ZHANG J., LIU Y.M., ZHANG L. The Beijing climate center climate system model (BCC-CSM): the main progress from CMIP5 to CMIP6. *Geoscientific Model Development*, **12**, 1573, **2019**.
35. ELITH J., PHILLIPS S.J., HASTIE T., DUDÍK M., CHEE Y.E., YATES C.J. A statistical explanation of MaxEnt for ecologists. *Diversity and Distributions*, **17**, 43, **2011**.
36. MUSCARELLA R., GALANTE P.J., SOLEY-GUARDIA M., BORJA R.A., KASS J.M., URIARTE M., ANDERSON R.P. ENMeval: An R package for conducting spatially independent evaluations and estimating optimal model complexity for Maxent ecological niche models. *Methods in Ecology and Evolution*, **5**, 1198, **2014**.
37. DARNIUS O., NORMALINA., MANURUNG A. Model selection in regression linear: a simulation based on akaike's information criterion. *Journal of Physics: Conference Series*, **1321**, 022085, **2019**.
38. WARREN D.L., SEIFERT S.N. Ecological niche modeling in Maxent: the importance of model complexity and the performance of model selection criteria. *Ecological Applications*, **21**, 335, **2011**.
39. MORALES N.S., FERNÁNDEZ I.C., BACA-GONZÁLEZ V. MaxEnt's parameter configuration and small samples: are we paying attention to recommendations? A systematic review. *PeerJ*, **5**, 2167, **2017**.
40. RADOSAVLJEVIC A., ANDERSON R.P. Making better Maxent models of species distributions: complexity, overfitting and evaluation. *Journal of Biogeography*, **41**, 629, **2014**.
41. BURNHAM K.P., ANDERSON D.R. Multimodel inference: understanding AIC and BIC in Model Selection. *Sociological Methods and Research*, **33**, 261, **2004**.
42. PHILLIPS S.J., ANDERSON R.P., SCHAPIRE R.E. Maximum entropy modeling of species geographic distributions. *Ecological Modelling*, **190**, 231, **2006**.
43. HUANG Y.S., AO Y., JIANG M.X. Reproductive Plasticity of an Invasive Insect Pest, Rice Water Weevil (Coleoptera: Curculionidae). *Journal of Economic Entomology*, **110**, 2381, **2017**.
44. SANGLE P.M., SATPUTE S.B., KHAN F.S., RODE N.S. Impact of Climate Change on Insects. *Trends in Biosciences*, **8**, 3579, **2016**.
45. FORREST J.R.K. Complex responses of insect phenology to climate change. *Current Opinion in Insect Science*, **17**, 49, **2016**.
46. KING M., ALTDORFF D., LI P., GALAGEDARA L., HOLDEN J., UNC A. Northward shift of the agricultural climate zone under 21st-century global climate change. *Scientific Reports*, **8**, 1, **2018**.
47. WOLDEAREGAY M., DEBRE BIRHAN UNIVERSITY DEPARTMENT OF BIOLOGY. Climate change impacts on the distribution and phenology of plants: A review. *Tropical Plant Research*, **7**, 196, **2020**.
48. SULTANA S., BAUMGARTNER J.B., DOMINIAC B.C., ROYER J.E., BEAUMONT L.J. Impacts of climate change on high priority fruit fly species in Australia. *PloS one*, **15**, 1932, **2020**.
49. KAMEL M., BREM A.S., MOURS Y.M.M., RAGAB S.H. Predicting the geographic distribution habitats of *Schizomyia buboniae* (Diptera: Cecidomyiidae) and its host plant *Deverra tortuosa* (Apiaceae) in Egypt by using MaxEnt modeling. *The Journal of Basic and Applied Zoology*, **82**, 1, **2021**.
50. WAN J., QI G.J., MA J., REN Y.L., WANG R., MCKIRDY S. Predicting the potential geographic distribution of *Bactrocera bryoniae* and *Bactrocera neohumeralis* (Diptera: Tephritidae) in China using MaxEnt ecological niche modeling. *Journal of Integrative Agriculture*, **19**, 2072, **2020**.
51. TEIXEIRA C.M., KRÜGER A.P., NAVA D.E., GARCIA F.R.M. Potential global distribution of the South American cucurbit fruit fly *Anastrepha grandis* (Diptera: Tephritidae). *Crop Protection*, **145**, 105647, **2021**.
52. GAO T., SHI J. The potential global distribution of *Sirex juvencus* (Hymenoptera: Siricidae) under near current and future climatic conditions as predicted by the maximum entropy model. *Insects*, **12**, 222, **2021**.
53. LEE C.M., LEE D.S., KWON T.S., ATHAR M., PARK Y.S. Predicting the global distribution of *Solenopsis geminata* (Hymenoptera: Formicidae) under climate change using the maxEnt model. *Insects*, **12**, 229, **2021**.
54. COBOS M.E., PETERSON A.T., BARVE N., OSORIO-OLVERA L. kuenm: an R package for detailed development of ecological niche models using Maxent. *PeerJ*, **7**, 2167, **2019**.
55. LI X.N., YE J.H. Meteorological data were used to predict the flight and spawning stages of rice water weevil in overwintering. *Plant Quarantine*, **6**, 330, **1998**.
56. ZHAI B.P., CHENG J.A., HUANG E.Y., SHANG H.W., ZHENG X.H., WU J., LV X.J. The oogenesis-flight syndrome of rice water weevil, *Lisorhoptrus oryzophilus* Kuschel. *Acta Ecologica Sinica*, **19**, 142, **1999** [In Chinese].
57. RON C., MICHAEL K., BOUAZZA S. Rice Water Weevil (Coleoptera: Curculionidae) Damage in Florida Rice Fields. *Journal of Entomological Science*, **51**, 219, **2016**.
58. PAN B.H., ZHENG Y., SHEN R.Q., YE T., ZHAO W.Z., DONG J., MA H.Q., YUAN W.P. High Resolution Distribution Dataset of Double-Season Paddy Rice in China. *Remote Sensing*, **13**, 4609, **2021**.
59. WEI J., CUI Y.L., LUO W.Q., LUO Y.F. Mapping Paddy Rice Distribution and Cropping Intensity in China from 2014 to 2019 with Landsat Images, Effective Flood Signals, and Google Earth Engine. *Remote Sensing*, **14**, 759, **2022**.
60. LING X.X., ZHANG Z.L., ZHAI J.Q., YE S.C., HUANG J.L. Global warming impacts on production and photosynthetic thermal productivity of rice in China. *Acta Agronomica Sinica*, **45**, 323, **2019** [In Chinese].